Optical properties of $TiFe_2O_4$ nanoparticles prepared by pulsed laser ablation in a liquid environment and their application in mercury removal.

Propiedades ópticas de las nanopartículas de $TiFe_2O_4$ preparadas mediante ablación láser pulsado en un ambiente líquido y su aplicación en la eliminación de mercurio.

Henry Riascos Landázuri[1]
Juan David López Vargas[2]
Johan Sebastián Duque Buitrago[3]

Abstract

Nanoparticles have garnered significant attention from researchers due to their enhanced properties compared to the same bulk materials. By reducing the material size, the contact area with the analyte increases exponentially, further enhancing the interaction between the sample and the target. This augmentation facilitates the acquisition of new and improved results. Titanium ferrite ($TiFe_2O_4$) is an alloy of particular interest to the scientific community. The amalgamation of a noble metal (Ti) with a metallic oxide forms a structure that combines the advantages of the metallic oxide with enhanced electrical conductivity due to the noble metal. This, in turn, expedites molecular interaction processes, reducing physical-chemical reaction

---

[1] Plasma, Láser y Aplicaciones, Universidad Tecnológica de Pereira, Profesor/investigador, hriascos@utp.edu.co

[2] Nanotechnology Engineering Research Program, Federal University of Rio de Janeiro, Brazil, estudiante/investigador, e-mail: juandlopezv94@gmail.com.

[3] Universidad Tecnológica de Uruguay, ITR-CS, Francisco Antonio Maciel s/n esq. Luis Morquio, Uruguay, Profesor/investigador, johan.duque@utec.edu.uy

times. In the current literature, limited information is available regarding the synthesis of $TiFe_2O_4$ nanoparticles, particularly through the pulsed laser ablation in liquid (PLAL) technique, known for its environmentally friendly approach to nanoparticle synthesis. With this context in mind, this work presents the synthesis and optical characterization of $TiFe_2O_4$ nanoparticles. $TiFe_2O_4$ nanoparticles were synthesized by PLAL technique, which consisted of the ablation of a $TiFe_2O_4$ target immersed in a beaker containing an aqueous solution, where one solution comprised water, and the other consisted of acetone. For nanoparticle synthesis, the pulse energy was kept at 50 mJ, while the aqueous solution, wavelength, and ablation time were varied. Once synthesized, the $TiFe_2O_4$ nanoparticles were characterized by ultraviolet visible (UV-Vis) spectroscopy to determine their optical properties. Using UVVis results, the localized surface plasmon resonance (LSPR) and band gap of each sample were determined, the latter using Tauc method. In a sample synthesized in water, for 20 minutes and using the wavelength of 532 nm, the LSPR was observed at 270 nm. On the other hand, for the sample synthesized in acetone using the same parameters, the LSPR was observed around 330 nm and 490 nm. In addition, an analysis of the evolution over time showed that $TiFe_2O_4$ nanoparticles were stable when synthesized in acetone, and unstable when synthesized in water due to nanoparticle decantation over time. Finally, mercuric chloride ($HgCl_2$) removal experiments on agar plates of these nanoparticles were performed and quantified by Atomic Absorption Spectroscopy, where it was possible to observe a percentage of $HgCl_2$ elimination of around 15%.

Keywords: $TiFe_2O_4$ nanoparticles; UV-Vis; localized surface plasmon resonance; pulsed laser ablation; mercury removal.

Resumen

Las nanopartículas han atraído la atención por parte de los investigadores debido a sus propiedades mejoradas en comparación con el mismo material a granel. Al reducir el tamaño del material, el área de contacto con el analito aumenta exponencialmente, mejorando aún más la interacción entre la muestra y el objetivo. Este aumento facilita la adquisición de resultados nuevos y mejorados. La ferrita de titanio ($TiFe_2O_4$) es una aleación de especial interés para la comunidad científica. La unión de un metal noble (Ti) con un óxido metálico forma una estructura que combina las ventajas del óxido metálico con una conductividad eléctrica mejorada debido al metal noble. Esto, a su vez, acelera los procesos de interacción molecular, reduciendo los tiempos de reacción físico-química. En la literatura actual, hay información limitada disponible sobre la síntesis de nanopartículas de $TiFe_2O4$, particularmente a través de la técnica de ablación por láser pulsado en líquido (PLAL), conocida por su enfoque amigable con el medio ambiente para la síntesis de nanopartículas. Teniendo en cuenta este contexto, este trabajo presenta la síntesis y la caracterización óptica de nanopartículas de $TiFe_2O_4$. Las nanopartículas de $TiFe_2O_4$ se sintetizaron mediante la técnica de ablación láser pulsada en líquido (PLAL), que consistió en la ablación de un objetivo de $TiFe_2O_4$ sumergido en un vaso que contenía una solución acuosa, una con agua y la otra con acetona. Para la síntesis de las nanopartículas, se mantuvo la energía del pulso en 50 mJ, mientras que se variaron la solución acuosa, la longitud de onda y el tiempo de ablación. Una vez sintetizadas, las nanopartículas de $TiFe_2O_4$ se caracterizaron mediante espectroscopía ultravioletavisible (UV-Vis) para determinar sus propiedades ópticas. Utilizando los resultados de UVVis, se determinaron la resonancia plasmónica superficial localizada (LSPR, por sus siglas en inglés) y la banda prohibida de cada muestra, esta última utilizando el método de Tauc. En la muestra sintetizada en agua durante 20 minutos y utilizando una longitud de onda de 532 nm, se observó LSPR a 270 nm. Por otro lado, en la muestra sintetizada en acetona utilizando los mismos parámetros, se observó LSPR alrededor de 330 nm y 490 nm. Además, un análisis de la evolución a lo largo del tiempo mostró que las nanopartículas de $TiFe_2O_4$ eran estables cuando se sintetizaban en acetona, e inestables cuando se sintetizaban en agua debido a la decantación de las nanopartículas con el tiempo. Por último, se realizaron experimentos de eliminación de cloruro mercúrico ($HgCl_2$) en placas de agar con estas nanopartículas y se cuantificaron mediante espectroscopía de absorción atómica, donde fue posible observar un porcentaje de eliminación de $HgCl_2$ de alrededor del 15%.

Palabras clave: Nanopartículas de $TiFe_2O_4$; UV-Vis; resonancia plasmónica superficial localizada; ablación láser pulsado; eliminación de mercurio.

1. Introduction

Metal nanoparticles (MNPs) have garnered the attention of scientists due to their enhanced optical properties that strongly depend on the size, shape, concentration, refractive index of the material, and surrounding media (ElFaham et al., 2021; Shnoudeh, et al., 2019; Shukla et al., 2017). These enhanced properties of MNPs have been explored and implemented in several applications, such as biosensors, drug delivery systems, and photocatalyst processes, among others (Guo et al., 2022; Altowyan et al., 2021; Khudiar et al., 2021; Lopez et al., 2021; Zhang et al., 2014).

Among the MNPs, metallic oxides have been more extensively explored in recent years due to their lower cost when compared to noble metals such as gold and silver, and also because it increases the range of applications. A property of metallic oxides on the nanoscale is that, when interacting with light, they exhibit improved electrical and photonic properties compared to their respective properties at the macroscale. As a result of the interaction between metal oxide nanoparticles and light, oscillation modes localized surface plasmon resonances (LSPR) are generated. These are collective oscillations of electrons (electronic plasma) at the metal-dielectric interface (Kochuveedu et al., 2013; Sekhon, et al., 2011).

Recently, metal oxide nanoparticles based on titanium ferrite (TiFeO), also known as spinels, have been used frequently for application in photo-catalyst processes such as dye degradation, air cleaning, and heavy metal removal. These TiFeO nanoparticles exhibited good photocatalytic activities under UV irradiation and can be recycled multiple times by magnetic separation without significant loss of activity, as reported by Shukla et al. (2017). TiFeO nanoparticles have proven to be a promising material for contaminated groundwater treatment and might open a new way for the design of cheaper and more efficient largescale water purification plants, as reported in recent literature (Maksoud et al., 2020; Lais et al., 2018). TiFeO has practical application as a heterogeneous catalyst for the effective removal of textile dyes commonly found in wastewater (Ramalho *et al.*, 2021). The strong bonds within these dye chains make their elimination challenging during water treatment. However, TiFeO exhibits promising effectiveness in this regard, demonstrating nearly 100% efficiency in dye removal during bench tests. Notably, its ability to be reused adds to its significance in addressing water treatment challenges. In the last decade, TiFeO has been combined with cobalt, nickel, zinc, and other materials to enhance its magnetic and optical properties (Khalid et al., 2023; Li et al., 2021; Amaliya et al., 2018). While this mixture has shown improved characteristics, there are still certain properties of TiFeO that require further investigation before it can be effectively utilized in conjunction with other materials.

An important analysis of the nanoparticles synthesized by the Pulsed Laser Ablation in Liquid (PLAL) technique is to determine its band gap energy because it is related to the localized surface plasmon resonance (LSPR). This property of MNPs allows the application of TiFeO nanoparticles in photocatalytic processes for pollutant degradation, as reported by Abdeltif et al. (2022) and Amrane et al. (2020), hence the importance of band gap modification and LSPR tuning of a nanomaterial according to the synthesis method (Leong et al., 2018; Zhang et al., 2017; Shukla et al., 2017).

Among the most commonly used synthesis methods for the production of nanoparticles, we can mention Sol-Gel and evaporation, both chemical methods that require several dangerous chemical precursors, which contaminate the final product and limit its biological applications. In contrast, PLAL is a fast, green, onestep physical approach, where a solid target is ablated at the solid-liquid interface under liquid confinement. This high-temperature and high-pressure non-equilibrium processing is used to produce a colloidal solution of high-quality nanoparticles and/or thin films (Sportelli et al., 2018; Pérez et al., 2015; Mahdieh et al., 2015; Nikolov et al., 2012).

In this work, we present the synthesis of nanoparticles from a $TiFe_2O_4$ target in different liquid environments, varying the laser wavelength and ablation time. The properties of the synthesized nanoparticles were characterized by Ultraviolet-visible (UV-Vis) spectroscopy, with which the energy band gap and the localized surface plasmon resonance (LSPR) were estimated, focusing on their application in the removal of dissolved mercuric chloride ($HgCl_2$). In addition, $HgCl_2$ removal tests were quantified using Atomic Absorption Spectroscopy (AAS) in Nutrient Agar Plates experiments.

2. Experimental details

Figure 1 shows the PLAL experimental schematic used for the syntheses of $TiFe_2O_4$ nanoparticles. Under experimental conditions, we used two Q-switched Nd:YAG nanosecond pulsed laser systems, one operated at the fundamental wavelength (1064 nm) and the other at wavelength 532 nm, with 10 Hz and 20 Hz of repetition rates, respectively. The pulse duration of both lasers is 9 ns, and both were used with a pulse energy of 50 mJ. The experimental setup employed closely follows the methodology reported by Cuenca et al. (2022); Lopez et al. (2021); Duque et al. (2019), and Pérez et al. (2015). However, a notable distinction lies in the choice of the target material, specifically TiFe2O4, and, more significantly, its applicability to mercury removal in this particular case.

Titanium ferrite nanoparticles ($TiFe_2O_4$) were obtained from a solid $TiFe_2O_4$ target, which was placed inside a beaker and immersed in 10 ml of a liquid medium at room temperature. For this study, we used acetone and double-distilled water as the liquid medium. The target surface was immersed in 2 mm of liquid for all the syntheses performed in this work. The laser fluence was 0.98 J/cm^2 for wavelengths of 1064 nm and 1.16 J/cm^2 for 532 nm. During synthesis, the target was ablated for 10 or 20 minutes depending on the defined experimental condition. Varying the solvent and wavelength parameters enables the modification of the nanoparticles' optical properties, aligning with the objectives of this study. Conversely, changes in the ablation time solely impact the quantity and size of the synthesized nanoparticles. After each synthesis, the target experienced a weight loss ranging from 0.05 to 0.10 grams, facilitating the conduction of numerous experiments without altering the initial matrix. Table I provides a summary of the experimental conditions for the synthesis of each sample, with each sample enumerated.

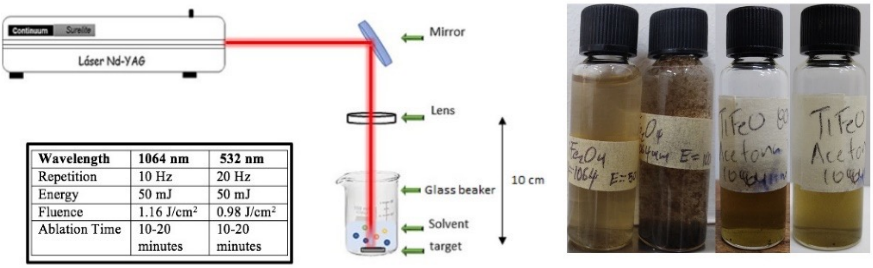

Wavelength	1064 nm	532 nm
Repetition	10 Hz	20 Hz
Energy	50 mJ	50 mJ
Fluence	1.16 J/cm²	0.98 J/cm²
Ablation Time	10-20 minutes	10-20 minutes

Fig. 1. *Pulsed laser ablation in liquid technique used for the synthesis of* $TiFe_2O_4$ *nanoparticles.*

TABLE I

$TIFE_2O_4$ NANOPARTICLES PREPARED BY PULSED LASER ABLATION IN LIQUID

#	Medium	Wavelength	Time ablation	Energy
1	Acetone	1064 nm	10 min	50 mJ
2	Acetone	1064 nm	20 min	50 mJ
3	Acetone	532 nm	10 min	50 mJ
4	Acetone	532 nm	20 min	50 mJ
5	Water	1064 nm	10 min	50 mJ
6	Water	1064 nm	20 min	50 mJ
7	Water	532 nm	10 min	50 mJ
8	Water	532 nm	20 min	50 mJ

A Thermo Scientific Evolution® (201/220 series, USA) spectrometer was used to study the optical properties of $TiFe_2O_4$ nanoparticles in the UV-Vis Spectrum, with quartz cuvettes of a one-centimeter optical path.

For $HgCl_2$ removal experiments, a standard Hg solution with 8ppm at 89.89% was deposited on Nutrient Agar Plates with 1 mL of $TiFe_2O_4$ nanoparticles. The $HgCl_2$ removed by $TiFe_2O_4$ nanoparticles was analyzed by atomic absorption spectroscopy with a Thermo Solar S4 Atomic Absorption Spectrophotometer using an Hg lamp at 253.7 nm in BGC-D2 mode with a slit width of 0.7 nm.

3. Results and discussion

3.1. UV-Vis analysis

Several sets of nanoparticles were synthesized from a solid $TiFe_2O_4$ target using the PLAL technique, varying parameters such as ablation time, liquid environment, and laser wavelength (conditions detailed in Table 1). To determine the effect of the synthesis conditions on the nanoparticles, the optical absorbance spectra were analyzed.

Figures 2a and 2b display the UV-Vis absorbance spectra of the nanoparticles for two ablation times and three different aging durations. In all instances, a distinct absorbance band is evident in the visible region. The optical spectra of nanoparticles synthesized in acetone, employing a wavelength of 1064 nm, pulse energy of 50 mJ, and an ablation time of 10 minutes for deposition, are depicted in Figure 2a. This figure also illustrates the progression of absorbance concerning aging time, with analyses conducted at 0, 14, and 21 days. The spectra clearly show two absorbance bands, one at 339 nm (UV region) and the other at 442 nm (visible region), which are characteristic absorbance spectra of titanium dioxide and iron oxide in the ultraviolet and visible regions (Shukla et al., 2015; Chen et al., 2007). The strong absorption in the UV region is due to the dd electronic transition between the Ti^{4+} ion and the O_2 ligand of the anatase phase of the TiO_2 compound, while the band at 442 nm (visible region) is attributed to iron oxide (Shukla et al., 2015; Chen et al., 2007).

No shift is observed in the absorption edge (UV region) of the nanoparticles during the aging process, indicating that the nanoparticles synthesized in acetone are stable. However, the absorption intensity decreases with the nanoparticles' aging process, which means that immediately after ablation, the nanoparticles have a higher oxidation state. On the other hand, the absorption peak in the visible region shows a slight red shift during the aging process, which can be attributed to a charge transfer transition between the d electrons of iron and the conduction or valence band of TiO_2.

The absorbance spectra shown in Figure 2b are of the $TiFe_2O_4$ nanoparticles synthesized with 20 minutes of ablation and in the same conditions as the sample shown in Figure 2a. It can be seen that the absorption edge of the nanoparticles just after ablation is smaller than the absorption edge of the sample synthesized within 10 minutes of ablation, which indicates indirectly that the nanoparticles formed are a smaller size oxide (Ismail et al., 2021; Khan et al., 2016; Hamad et al., 2016).

Regarding the aging time, no significant shift is observed in the absorbance spectra for 10- and 20-min ablation times (in acetone), which means that there is probably little agglomeration of nanoparticles and that the size of the nanoparticles does not depend on the aging time. However, the absorption peak at 442 nm during 20 min of ablation shows a broadening and a lower intensity, indicating that the size distribution of nanoparticles increases with the aging time (Hamad et al., 2016; Zeng et al., 2012; Schwenke et al., 2011).

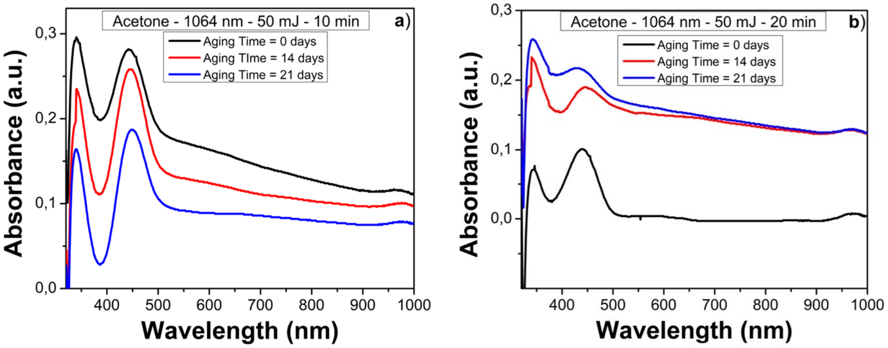

Fig. 2. *TiFe2O4 nanoparticles synthesized in acetone using a wavelength of 1064 nm and pulse energy of 50 mJ; (a) 10 min of ablation, and (b) 20 minutes of ablation.*

Figure 3 shows the UV-Vis spectra of the nanoparticles synthesized in deionized water using the wavelength 1064 nm, pulse energy 50 mJ, and, 10- and 20- min times ablation. These spectra show that the absorbance of the nanoparticles decreases and there is also a shift to lower wavelengths (blue shift) with increasing aging time. This change in absorbance is more evident for the sample prepared in 10 min ablation (see Fig. 3a). In addition, the absorbance edge begins in the visible region and decreases with aging time, which indicates that the size of the nanoparticles is smaller at 21 days after ablation, furthermore, agglomerations are not evident in the colloid. On the other hand, the absence of the absorbance peak around 400 nm, which appears in the spectra of the nanoparticles formed in acetone, is probably due to bimetallic nanoparticles (Ti-Fe-O) with the incorporation of the ion Fe^{+3}/Fe^{+4} and no formation of iron oxide (Shukla et al., 2017; Khan et al., 2016; Shukla et al., 2015).

Optical absorbance spectra of $TiFe_2O_4$ nanoparticles produced in acetone and using a wavelength of 532 nm are shown in Figure 4a (10 min of ablation) and in Figure 4b (20 min ablation). The characteristic band of $TiFe_2O_4$ nanoparticles is observed at 335 nm (very intense) and the band corresponding to iron oxide is located at 490 nm (blue color curve), perfectly defined 14 days after ablation. Comparing the two samples synthesized using the wavelength of 532 nm with that of 1064 nm, it can be said that the absorbance is more intense when synthesized with 532 nm, and the iron oxide band has a redshift and is weaker. The difference in intensities can be attributed to a greater amount of $TiFe_2O_4$ nanoparticles. Likewise, the shift of the LSPR to longer wavelengths indicates the formation of larger $TiFe_2O_4$ particles, which improve its spherical structure (Khan et al., 2016; Shukla et al., 2015; Chen et al., 2007).

According to the Beer-Lambert law structure (Dariani et al., 2016; Yan et al., 2012), there is a linear relationship between absorbance and concentration, thus, a higher concentration of nanoparticles leads to a higher absorbance value, and it can result in a more stable suspension. For nanoparticles in suspension with low stability, the absorbance is low due to nanoparticle agglomeration. With the above, we can conclude that when the nanoparticles are synthesized using the wavelength of 1064 nm, they presented fewer agglomerations.

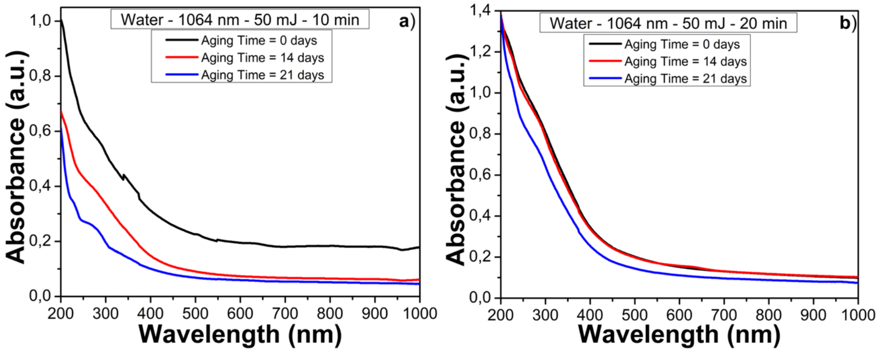

Fig. 3. *$TiFe_2O_4$ nanoparticles synthesized in deionized water using a wavelength of 1064 nm and pulse energy of 50 mJ; (a) 10 minutes of ablation, and (b) 20 minutes of ablation.*

Figure 5 shows UV–vis spectra of the $TiFe_2O_4$ nanoparticles prepared using 532 nm wavelength in deionized water. Similar to the spectra shown in Figure 3, the LSPR of TiO appears around 270 nm, but the LSPR of Fe is absent. The strong iron oxide/water coordination alters the nanoparticle surface characteristic, leading to damping of the LSPR peak. It is known that the interaction of the metal surface, having a partially filled conduction band with solvents containing p-bonds leads to significant damping of LSPR/SPR compared to solvents that do not contain p-bonds. Delocalized p-bond electrons in the solvent molecules can contribute electron density to the Ti surface, thus reducing the density of free electrons in the conduction band and damping the plasmon oscillations.

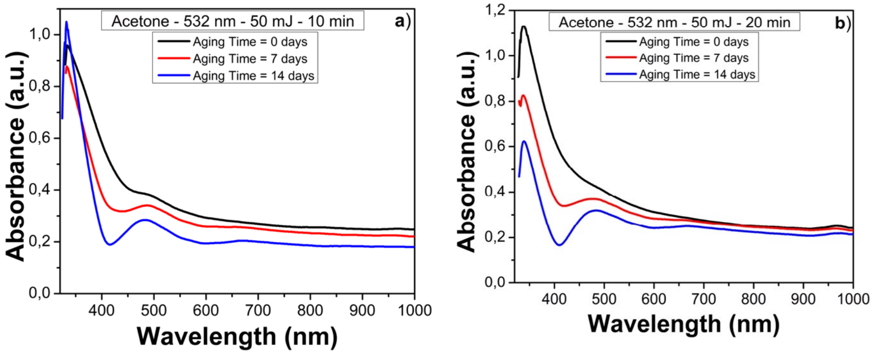

Fig. 4. *$TiFe_2O_4$ nanoparticles synthesized in acetone using a wavelength of 532 nm and pulse energy of 50 mJ; (a) 10 minutes of ablation, and (b) 20 minutes of ablation.*

The LSPR can be influenced by the material, size, shape, and surrounding medium of nanoparticles (solvent, ligands), as well as interparticle spacing. In bimetallic particles, the LSPR depends further on the composition and the distribution of the two metals (Ismail et al., 2021).

On the other hand, the increase in LSPR intensity in the spectra of Figure 5 compared to the spectra of Figure 3, indicates a reduction of the metal ions. This suggests that the position of the LSPR band of $TiFe_2O_4$ alloy system depends on the relative concentrations of TiO and Fe along with the duration of exposure and irradiation energy.

Finally, in optical absorbance spectra of nanoparticles synthesized in deionized water (Figures 3 and 5), a single peak was observed, so this result suggests that the sample consists of bimetallic nanoparticles and there is neither a mixture nor a core/shell.

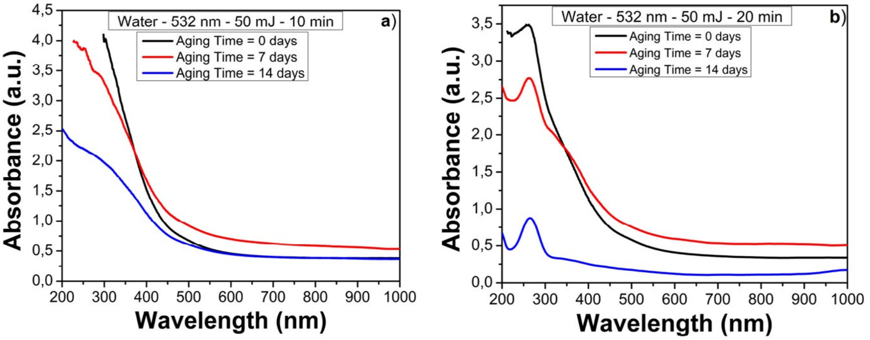

Fig. 5. *$TiFe_2O_4$ nanoparticles synthesized in deionized water using a wavelength of 532 nm and pulse energy of 50 mJ; (a) 10 minutes of ablation, and (b) 20 minutes of ablation.*

3.2. Band gap estimation

From the absorbance spectra, the energy band gap of the studied samples was evaluated. $TiFe_2O_4$ nanoparticles are considered a direct bandgap material, n = 1/2. Consequently, the absorption coefficient can be described by the expression (Akshay et al., 2019):

$$(\alpha\hbar\nu)^{(1/2)} = \hbar\nu - E_{gap} \tag{1}$$

where α is the absorption coefficient, ħ is the Planck constant and ν the frequency. The zeros of equation (1) appear when $E_{gap} = \hbar\nu$.

This equation was programmed so that its input set was the UV-Vis data, and the output was the Tauc plot with the E_{gap} value. The band gap of each material determined from the UVVis spectra is presented in Table II.

Depending on the synthesis conditions of each sample, the band gap values obtained by Tauc plot method were between 1.01 and 2.66 eV, whereas the estimated errors are within ±0.20 eV. The highest band gap values correspond to the samples prepared in acetone using the wavelength of 532 nm. The samples prepared in water presented lower band gap values for both laser wavelength.

Performing a comparative analysis with the band gap of TiO_2 nanoparticles (> 3.19 eV) (Saranya et al., 2018), the bandgap of the samples synthesized in this work was smaller. Additionally, the absorbance edge presented a redshift that is attributed to the charge-transfer transition between the iron oxide electrons and the TiO_2 conduction band (Ismail et al., 2021). Although the Fe ions in TiO_2 do not change the position of the edge of the TiO_2 valence band, it introduces new energy levels of transition Fe ions in the TiO_2 band gap and causes absorbance in the visible region.

TABLE II
BAND GAP VALUES OF $TIFE_2O_4$ NANOPARTICLES PREPARED BY PULSED LASER ABLATION IN LIQUID.

#	Medium	Wavelength	Time ablation	Band gap
1	Acetone	1064 nm	10 min	2.03 eV
2	Acetone	1064 nm	20 min	2.06 eV
3	Acetone	532 nm	10 min	2.66 eV
4	Acetone	532 nm	20 min	2.47 eV
5	Water	1064 nm	10 min	1.55 eV
6	Water	1064 nm	20 min	1.82 eV
7	Water	532 nm	10 min	1.50 eV
8	Water	532 nm	20 min	1.01 eV

3.3. $HgCl_2$ Removal test

Metal oxides have been proposed to remove heavy metals (such as $HgCl_2$) from water due to their ease of recovery and regeneration, between these oxidized metals TiO_2 and Fe_3O_4 (Asgari et al., 2018; Dave et al., 2014). From the above, it is expected that the alloy between titanium dioxide and iron oxide will also be able to remove heavy metals.

Table III shows the Atomic Absorbance Spectroscopy (AAS) results for the target concentration of $HgCl_2$ at 89.89%. Experiments of removal were performed for samples of $TiFe_2O_4$ nanoparticles synthesized using the wavelengths 1064 nm and 532 nm, with pulse energy of 50 mJ, time ablation of 10 and 20 min, and in acetone.

The AAS results showed that the percentage of $HgCl_2$ removed was between 15.0% and 16.6%, being more significant for the $TiFe_2O_4$ nanoparticles synthesized at the wavelength of 1064 nm. If the band gap results are related to the $HgCl_2$ removal results, we can say that when the band gap was smaller, the highest $HgCl_2$ removal was obtained. The $HgCl_2$ removal tests were only performed for the samples synthesized in acetone since they presented stability over time, while the samples synthesized in distilled water presented instability and it decanted.

TABLE III
ATOMIC ABSORBANCE SPECTROSCOPY RESULT OF $HGCL_2$ REMOVAL.

#	Wavelength	Time ablation	Concentration (μg/L)	Absorbance
1	1064 nm	10 min	76.05	2.73
2	1064 nm	20 min	74.89	2.69
3	532 nm	10 min	76.40	2.74
4	532 nm	20 min	76.15	2.74

4. Conclusions

In summary, the synthesis of $TiFe_2O_4$ nanoparticles by pulsed laser ablation in liquid technique was carried out. Subsequently, the nanoparticles were characterized by UV-Vis spectroscopy and, finally, their $HgCl_2$ removal properties were studied.

Using UV-Vis spectroscopy, it was observed the absorbance spectra were more defined using the laser wavelength of 532 nm, which showed a better quality of the manufactured nanoparticles. The localized surface plasmon resonance of the nanoparticles was observed around 270 nm for sample synthesized using the wavelength 532 nm, ablation time of 20 min, and in distilled water, which indicates the homogeneous formation of $TiFe_2O_4$ nanoparticles. Likewise, it was observed around 330 nm and 490 nm when synthesized in an acetone environment, for both laser wavelengths, indicating the formation of colloidal $TiFe_2O_4$ nanoparticles and other species such as TiO_2.

The optical evolution over time analysis shows that the $TiFe_2O_4$ nanoparticles were stable when synthesized in acetone since colloids do not crowd or rush, unlike those nanoparticles produced in water which agglomerate and precipitate rapidly.

The nanoparticles' band gap was calculated using the Tauc plot method, obtaining values between 1.01 and 2.66 eV. For colloids in acetone, the band gap was smaller when the sample was synthesized using the wavelength of 532 nm. However, for the colloids in water, the opposite occurred, the bandgap was smaller when synthesized using the wavelength of 532 nm.

The $HgCl_2$ removal results show that with the use of $TiFe_2O_4$ nanoparticles synthesized in an acetone medium, there was a removal between 15.0% and 16.6% of $HgCl_2$.

These findings represent a noteworthy addition to the body of literature on $TiFe_2O_4$ synthesized via PLAL. Currently, there is a scarcity of studies that explore the synthesis technique's compatibility with this specific target. The enhanced optical properties observed in TiFe3O4, in comparison to pure iron oxide, position it as a promising candidate for applications in both biological and sensing domains. The improved optical characteristics have the potential to significantly impact molecular interaction mechanisms, expediting and facilitating interactions that may be challenging with iron oxide alone.

5. Acknowledgements

This work was supported by research project 3-23-1 from Universidad Tecnológica de Pereira, Colombia.

References

Abdeltif, A., Assadi, A., Nguyen-Tri, P., Nguyen, T.A., Rtimi. S. (2022). Nanomaterials for Air Remediation - 1st Edition. Elsevier.

Akshay, V.R., Arun, B., Mandal, G., Chanda, A., & Vasundhara, M. (2019). New Journal of Chemistry 43, (15).

Altowyan, A.S., Mostafa, A.M., & Ahmed, H.A. (2021). Optik 241 167217.

Amaliya, A. P., Anand, S., & Pauline, S. (2018). Journal of Magnetism and Magnetic Materials, 467, 14-28.

Amrane, A., Mohan, D., Nguyen, T. A., Assadi, A.A., Yasin, & G. (2020). Sorbents Materials for Controlling Environmental Pollution Chapter 26, 701-723. Elsevier.

Asgari Lajayer, B., Najafi, N., Moghiseh, E., Mosaferi, M., & Hadian, J. (2018). Journal of Nanostructure in Chemistry 8(4) 483-496.

Chen, X., Mao, S.S. (2007). Chemical Reviews 107(7) 2891-2959.

Cuenca, J.P., Lopez, J.D., Werneck, M.M., Camargo, S.S., Duque, J.S., & Riascos, H., (2022). Brazilian Journal of Physics 52(3) 1-8.

Dave P.N. & Chopda L.V. (2014). Journal of Nanotechnology, 398569.

Dariani, R. S., Esmaeili, A., Mortezaali, A., & Dehghanpour, S. (2016). Optik 127(18) 7143-7154.

Duque, J.S., Yandy, A.M., & Riascos, H. (2019). Journal of Physics: Conference Series 1247 (1).

ElFaham, M. M., Mostafa, A. M., & Toghan, A. (2021). Colloids and Surfaces A: Physicochemical and Engineering Aspects 630 127562.

Guo, R., Zhang, X., Liu, F., Huang, S., Yang, C., Li, H., & Lin, X. (2022). Physica Status Solidi (a) 219(9) 2200003.

Hamad, A., Li, L., & Liu Z. (2016). Applied Physics A 122(10) 1-15.

Ismail, M.A., Hedhili, M.N., Anjum, D.H., Singaravelu, V., Chung, S.H. (2021). Catalysts 11(4) 438.

Ismail, R.A., Erten-Ela, S., Ali, A. K., Yavuz, C., & Hassoon, K. I. (2021). Silicon 13(9) 3229-3237.

Khalid, K., Zahra, A., Amara, U., Khalid, M., Hanif, M., Aziz, M., ... & Abbas, W. (2023). Chemosphere, 338, 139531.

Khan, H., & Swati, I. K. (2016). Industrial & Engineering Chemistry Research 55(23) 6619-6633.

Khudiar, S.S., Nayef, U.M., & Mutlak, F.A.H. (2021). Optik 246 167762.

Kochuveedu, S.T., Jang, Y.H., & Kim, D.H. (2013). Chem. Society Rev.42 8467–8493.

Lais, A., Gondal, M.A, & Dastageer, M. A. (2018). Environmental Chemistry Letters 16(1) 183-210.

Leong, K. H., Abd-Aziz, A., Sim, L. C., Saravanan, P., Jang, M., & Bahnemann, D. (2018) Beilstein Journal of Nanotechnology 9(1) 628-648.

Li, J., Xu, T., Liu, L., Hong, Y., Song, Z., Bai, H., & Zhou, Z. (2021). Ceramics International, 47(13), 19247-19253.

Lopez, J.D., Keley, M., Dante, A., & Werneck M.M. (2021). Optical Fiber Technology 67 102731.

Mahdieh, M.H., & Fattahi, B. (2015). Applied Surface Science 329 47-57.

Maksoud, M. A., Elgarahy, A. M., Farrell, C., Ala'a, H., Rooney, D.W., & Osman, A.I. (2020). Coordination Chemistry Reviews 403 213096.

Nikolov, A. S, Nedyalkov, N.N., Nikov, R. G., Atanasov, P.A, Alexandrov,

& M.T., Karashanova, D.B. (2012). Applied Physics A 109(2) 315-322.

Pérez J. A., Riascos, H., & Vera, L.P. (2015). IEEE Sensors Journal 16(2) 359-364.

Ramalho, M. L. A., Madeira, V. S., Brasileiro, I. L. O., Fernandes, P. C., Barbosa, C. B., Arias, S., & Pacheco, J. G. A. (2021). Journal of Photochemistry and Photobiology A: Chemistry, 404, 112873.

Shnoudeh, A. J., Hamad, I., Abdo, R. W., Qadumii, L., Jaber, A.Y., Surchi, H.S., & Alkelany, S. Z. (2019). Biomaterials and Bionanotechnology pp. 527-612.

Sekhon, J.S., & Verma, S.S., (2011.) In Optical Instrumentation for Energy and Environmental Applications JWE22 Optical Society of America.

Shukla, A., Singh, S. C., Pandey, B.K., Uttam, K.N., Shah, J., Kotnala, R.K., & Gopal, R. (2015). Adv. Mater. Lett 6(12) 1066-1072.

Shukla, A., Bhardwaj, A. K., Pandey, B. K., Singh, S. C., Uttam, K. N., Shah, J., & Gopal, R. (2017). Journal of Materials Science: Materials in Electronics, 28, 15380-15386.